Supporting Information

Harnessing Peptide Binding to Capture and Reclaim Phosphate

Whitney C. Fowler,[†] Chuting Deng,[†] Gabriella M. Griffen,[†] O. Therese Teodoro,[†] Ashley Z. Guo,[†] Michal Zaiden,[§] Moshe Gottlieb,[*,§] Juan J. de Pablo,[*,†,‡] Matthew V. Tirrell[*,†,‡]

[†] Pritzker School of Molecular Engineering, University of Chicago, Chicago, Illinois 60637, United States,

[§] Chemical Engineering Department, Ben Gurion University, Beer Sheva 841050, Israel,

[‡] Argonne National Laboratory, Lemont, Illinois 60439, United States.

Keywords: Resource recovery, capture and release material, biomimetic material, phosphate recovery, computer simulations, free energy mapping

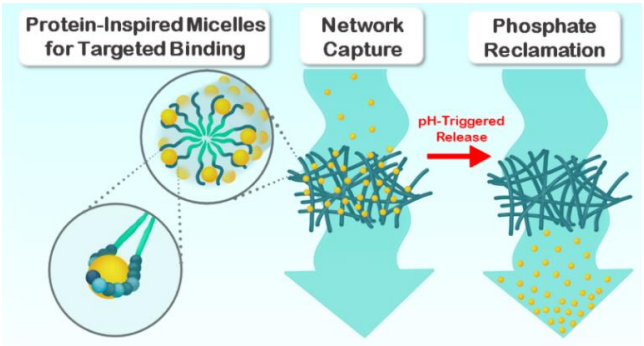

Table of Contents

1. Additional Experimental Results and Discussion

1.1 Mass Spectroscopy Verification using Matrix-Assisted Laser Desorption-Ionization – Time of Flight (MALDI-TOF)

The theoretical molecular weight for C_{16}GGGhex is 928.10 g/mol. The main peak in the purified HPLC fraction is 950.698 (Figure S1A). An artifact of this technique is that a sodium ion commonly adheres to the molecule in the place of a hydrogen atom upon ionization, making the detected mass larger than the mass of the molecule. After subtracting the molecular weight of a sodium ion (22.99 g/mol) and adding back the mass of the hydrogen atom it replaced, the confirmed molecular weight of C_{16}GGGhex is 928.72 g/mol. Similarly, for C_{16}SGKGHhex, the theoretical weight is 2288.55 g/mol. After subtracted the mass of sodium and adding the mass of hydrogen, the confirmed molecular weight of C_{16}SGKGHhex is 2287.37 g/mol (Figure S1B).

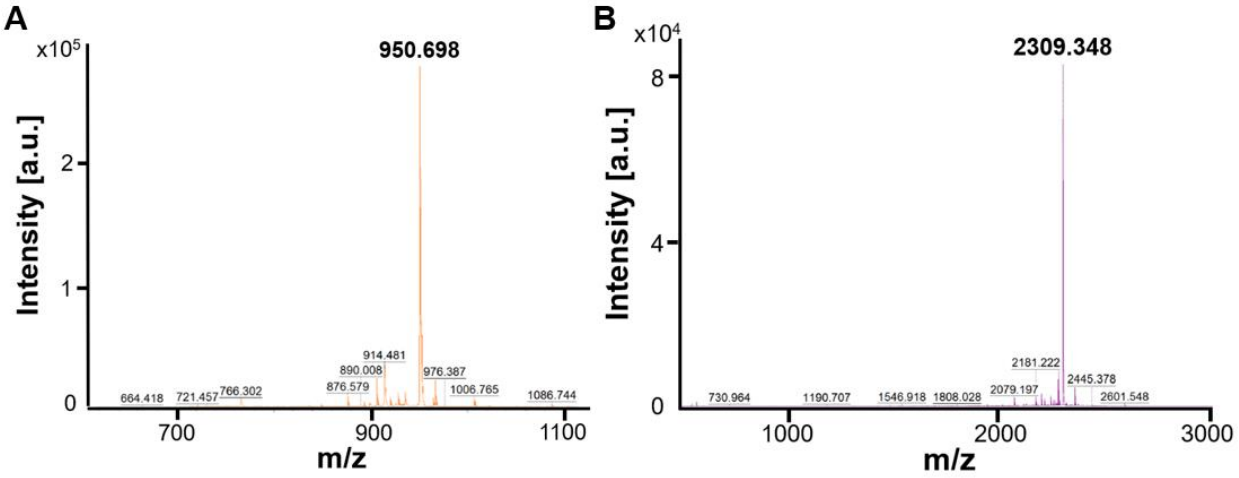

Figure S1. The mass spectra for (A) C_{16}GGGhex and (B) C_{16}SGKGHhex after purification from HPLC.

1.2 Purity Analysis using Liquid Chromatography – Mass Spectroscopy (LC-MS)

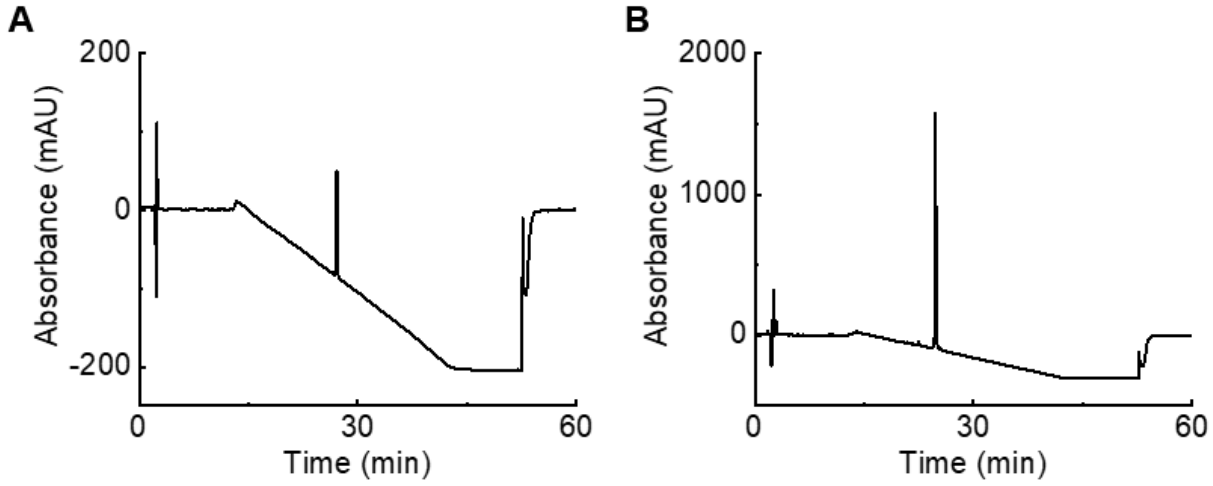

Figure S2. LC-MS chromatograph of (A) C_{16}GGGhex and (B) C_{16}SGKGHhex at 220 nm. The product elutes in the center peak for each plot. The purities were calculated to be (A) 96.5% and (B) 97.3%.

Table S1. LC-MS Chromatogram peak table for C_{16}GGGhex

Peak #	Ret. Time [min]	Area [mAU*s]	Height [mAU]	New Area [%]
1	7.075	17.42218	1.10176	1.81%
2	26.603	16.72878	1.79469	1.74%
3	**27.115**	**929.08282**	**134.86389**	**96.45%**
Total		19711.92	1744.347	100.00%

Table S2. LC-MS Chromatogram peak table for C_{16}SGKGHhex

Peak #	Ret. Time [min]	Area [mAU*s]	Height [mAU]	New Area [%]
1	15.06	71.84814	3.26691	0.36%
2	16.16	50.0343	3.10221	0.25%
3	17.457	16.36457	2.35443	0.08%
4	18.007	5.32924	1.11091	0.03%
5	18.234	33.99007	1.75981	0.17%
6	19.27	28.48297	4.28034	0.14%
7	19.704	12.98752	2.0538	0.07%
8	19.964	16.9283	2.95362	0.09%
9	20.449	30.83108	2.91836	0.16%
10	22.018	6.64445	1.70828	0.03%
11	22.312	5.37997	1.35502	0.03%
12	22.411	58.5399	15.22104	0.30%
13	22.538	63.15965	14.43723	0.32%
14	23.886	14.48648	1.14472	0.07%
15	**24.728**	**1.92E+04**	**1668.184**	**97.30%**
16	25.306	42.21921	7.38365	0.21%
17	25.446	12.94693	2.46567	0.07%
18	25.702	28.63228	4.45938	0.15%
19	26.481	8.51018	1.46951	0.04%
20	28.191	8.36704	1.13123	0.04%
21	29.378	15.93975	1.58721	0.08%
Total		19711.92	1744.347	100.00%

The confirmed purity of C_{16}GGGhex was 96.45%, and the confirmed purity of C_{16}SGKGHhex was 97.30%.

1.3 Critical Micelle Concentration (CMC)

The CMC is calculated as the inflection point of the fluorescence intensity beginning to increase, which occurs in the presence of hydrophobic cores (Figure S3). The CMCs were 8.43 μM and 130.1 μM for C16GGGhex and C16SGKGHhex, respectively. The ten-fold difference in CMC values can be explained by the packing parameter for surfactant molecules.[1] The packing parameter P evaluates the most stable degree of curvature at the tail-headgroup interface of the micelle using the ratio $P = v/al$, where (v) and (l) are the volume and maximum extended length of the tail, respectively, and (a) is the area of the headgroup at the interface. For C_{16}SGKGHhex, the (a) area of the headgroup is much larger due to the double-sided headgroup, causing each PA molecule to face more steric constraints in its ability to self-assemble, corresponding to the higher CMC. C_{16}SGKGHhex is also much more hydrophilic than C_{16}GGGhex with more than double the number of amino acids in the headgroup, further stabilizing the individual PA molecules in an unassembled state.

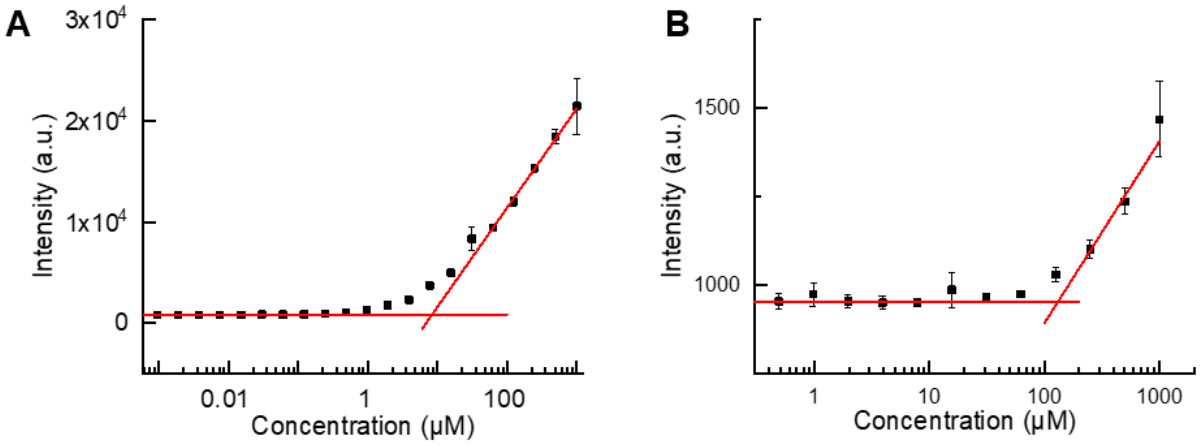

Figure S3. The CMC plots of (A) C_{16}GGGhex and (B) C_{16}SGKGHhex.

1.4 Additional Negative-Stain Transmission Electron Microscopy (TEM) Imaging

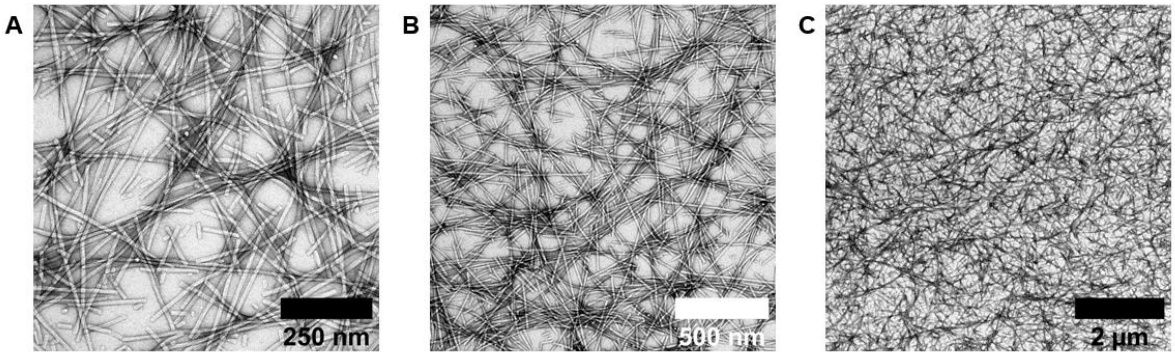

Figure S4. C_{16}GGGhex at pH 2 forms extended wormlike micelles.

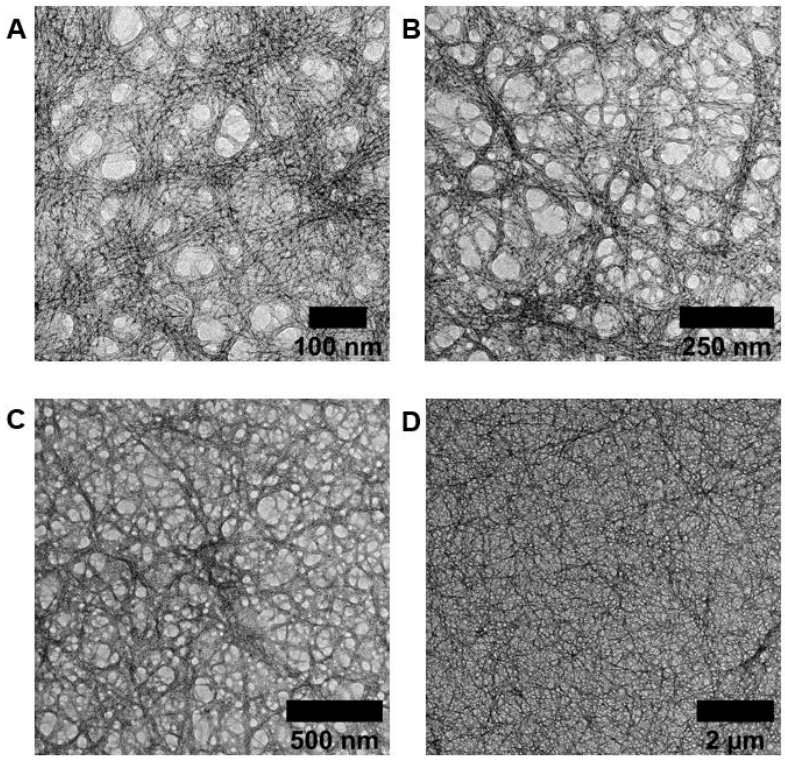

Figure S5. C_{16}GGGhex at pH 6 forms extended wormlike micelles.

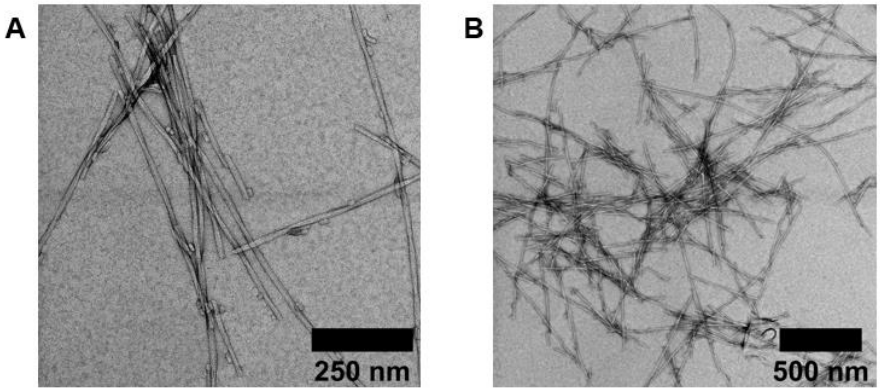

Figure S6. C_{16}GGGhex at pH 10 forms wormlike micelles that begin to clump together.

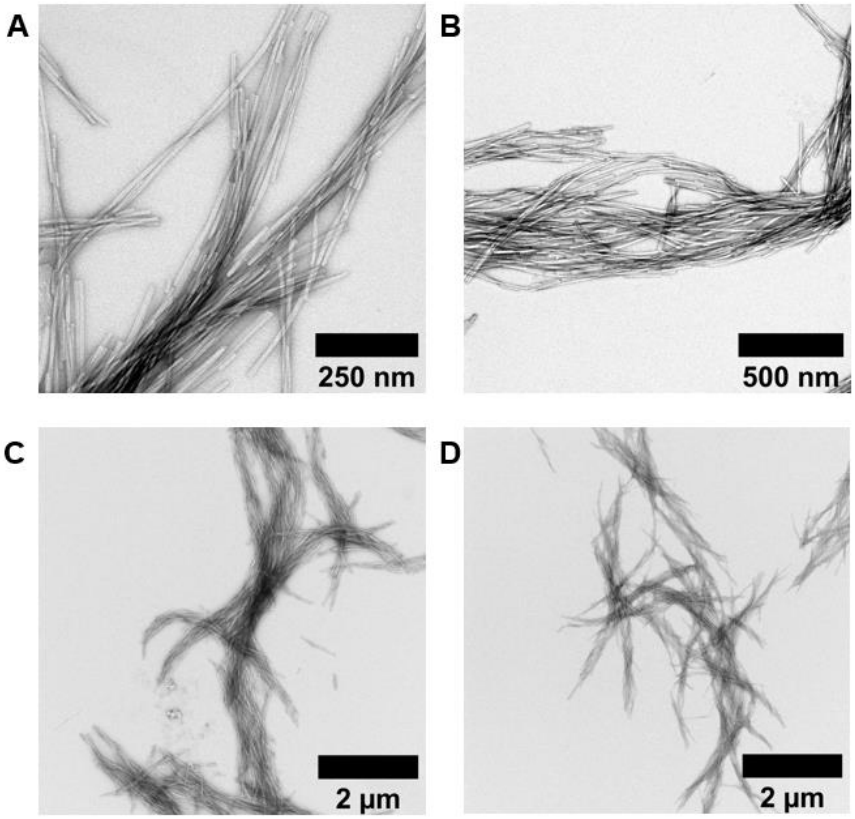

Figure S7. C_{16}GGGhex at pH 11 forms wormlike micelles that heavily clump together.

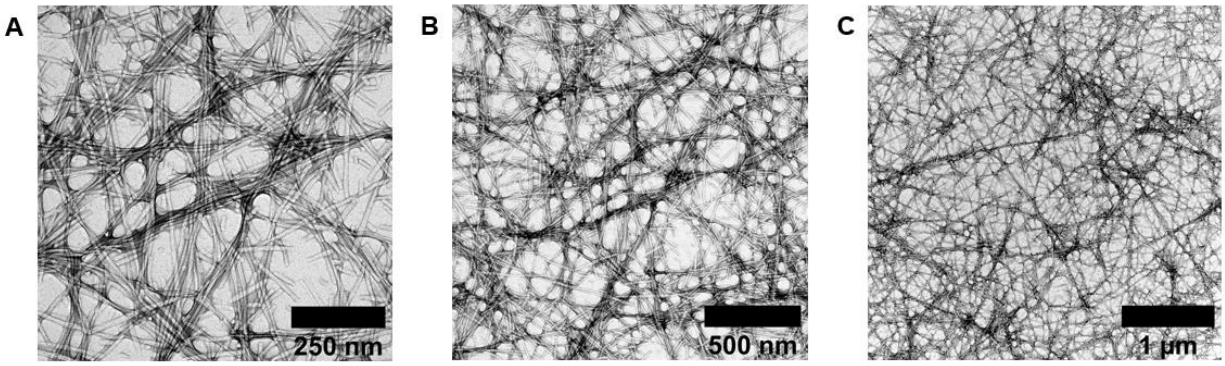

Figure S8. C_{16}GGGhex at pH 6 after one cycle of capture and release at pH 11 demonstrates that the declumping of the micelles is reversible.

For C_{16}SGKGHhex in Figure S9, this transition at high pH to wormlike micelles from spherical micelles can be understood in terms of the packing parameter discussed above. At low pH, the histidines are protonated, repelling each other and effectively increasing the area of the headgroup, pushing the packing parameter below the 1/3 value corresponding to spherical micelles to accommodate the larger steric hindrance. Upon deprotonation and a subsequent decrease in headgroup area at high pH, the assembly becomes more stabilized as wormlike micelles and approaches the 1/2 packing parameter value corresponding to the wormlike micelles seen in Figure S9.

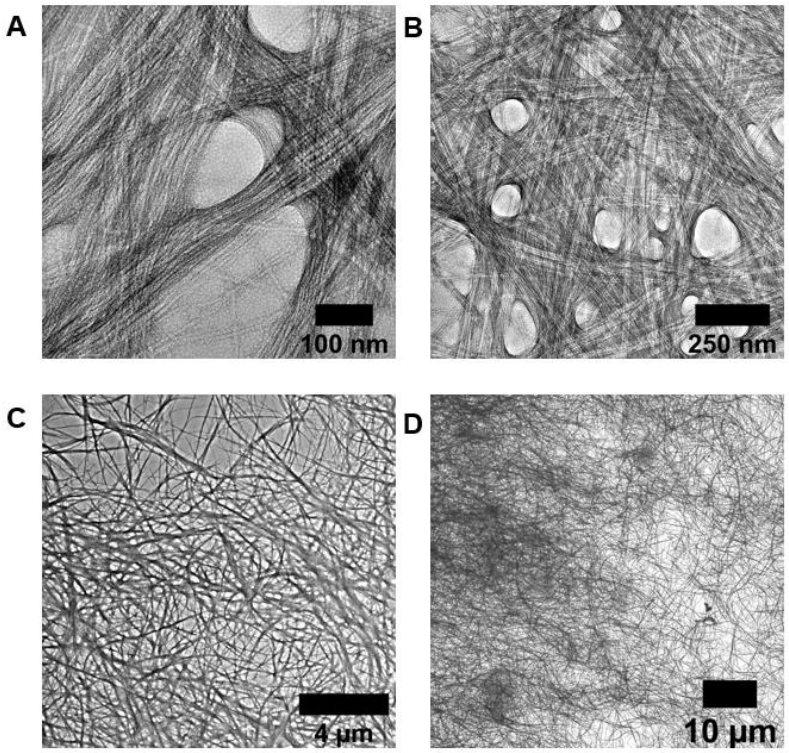

Figure S9. C_{16}SGKGHhex at pH 10 forms extended wormlike micelles that clump together very thickly.

1.5 Spectrophotometric Molybdenum Blue Assay

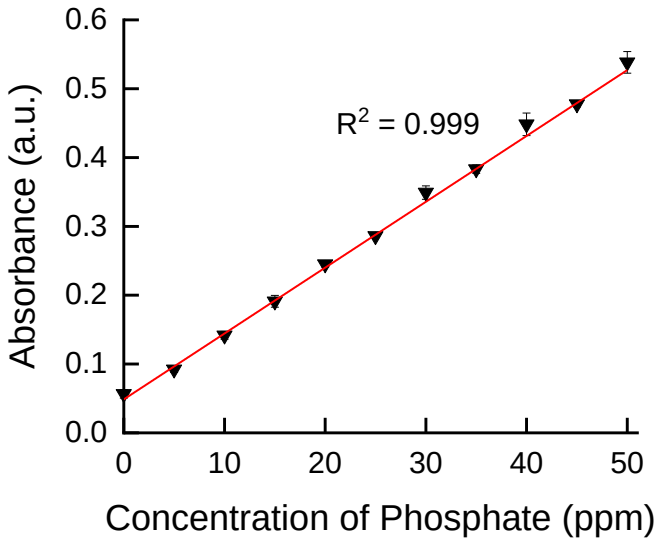

Figure S10. Confirmation of a linear trend using the spectrophotometric molybdenum blue assay. As concentration of phosphate in solution increases, the absorbance increases with very reliable accuracy.

1.6 Analysis of Kinetics of Binding

The kinetics data shown in Figure S11 demonstrated that C_{16}GGGhex sequestered and released phosphate within seconds to minutes of reaching the target pH, corresponding to the time it requires to promptly filter the suspension and evaluate the phosphate content. Additionally, the material maintains its unbound or bound state as long as the pH remains constant, up to the two hours that we tested

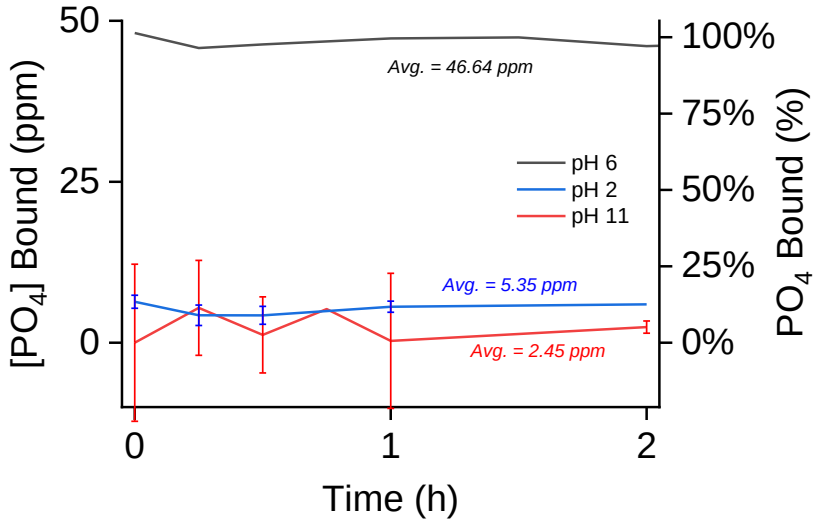

Figure S11. The phosphate binding concentrations and percentages measured over time at the three pH values of 6, 2, and 11. Phosphate is captured at pH 6 and unbound at pH 2 and 11 over the two hours measured.

1.7 Effect of Increased NaCl on Binding and the Molybdenum Blue Assay

As more NaCl is added to binding experiments of C_{16}GGGhex at pH 6, the amount of phosphate binding noticeably decreases (Figure S12). This phenomenon could explain the slight decrease in binding after multiple cycles of capture and release as the pH was repeatedly altered, if for example the wash steps between cycles did not completely wash out all NaCl and the concentration NaCl gradually accumulated in the sample as the number of cycles increases. This effect of decreased hexapeptide binding by an increase in NaCl concentration was also observed by Zhai, et al.[2]

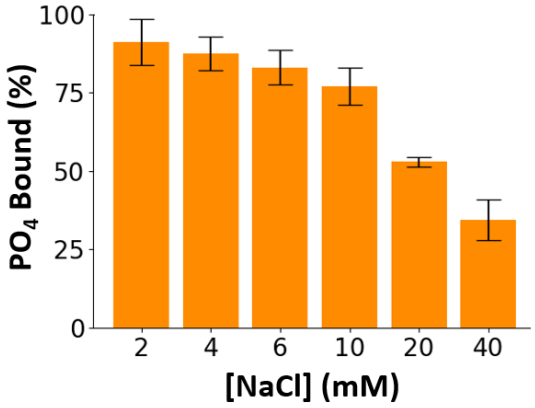

Figure S12. Binding experiments of C_{16}GGGhex at pH 6 at a 5:1 ratio of PA:PO_4 and varying final solution concentrations of NaCl.

We also investigated whether these higher concentrations affected the spectrophotometric assay to confirm that the observed decrease in binding was not an artifact of the assay (Figure S13). As the concentration of NaCl increases in the spectrophotometric calibration curves, the fitted lines do not noticeably vary or follow any noticeable trend, implying that added NaCl does not affect the spectrophotometric readings at these concentrations.

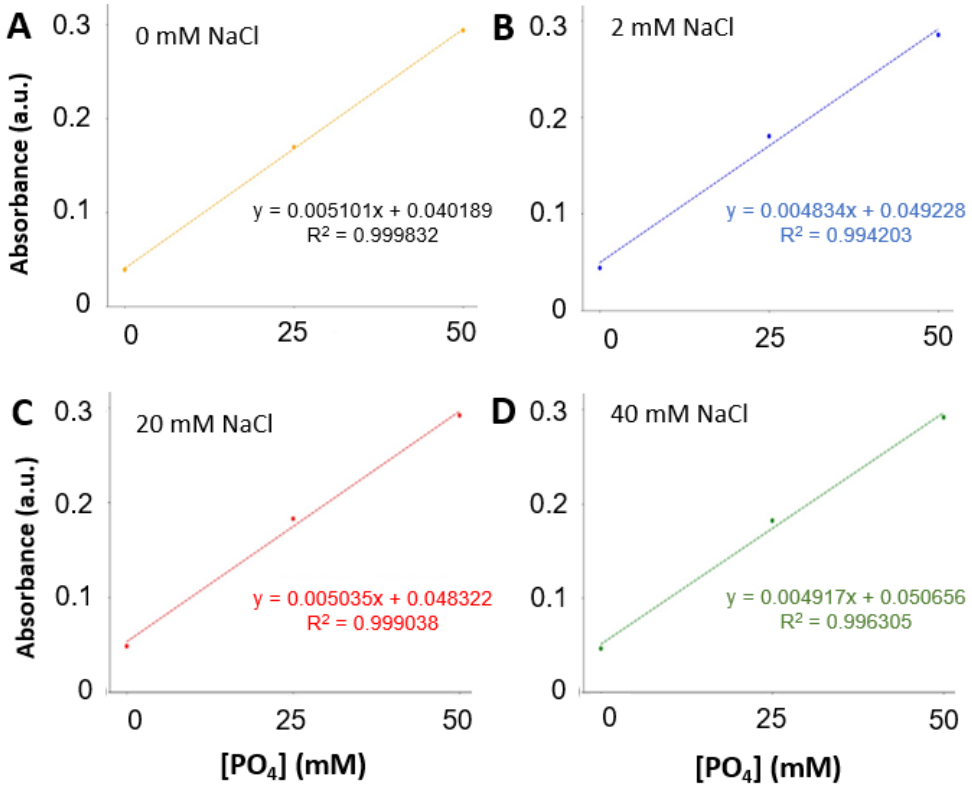

Figure S13. Spectrophotometric calibration curves constructed with increasing amounts of added NaCl, from (A) 0 mM NaCl, (B) 2 mM NaCl, 20 mM NaCl, and (D) 40 mM NaCl.

Even though we confirmed that binding is impacted by increased NaCl, the impact for our material is relatively small at the pH extremes. Table S3 details the average final concentration of added HCl and NaOH in order to achieve pH 2, 6, and 11 for our binding systems. The release conditions of pH 2 and 11 require concentrations of HCl and NaOH that fall in the range that would impact binding, both near 4 mM of added HCl or NaOH. However, this approximately 12% decrease in binding at pH 6 does not match the roughly 90-95% unbound phosphate at these extremes (Figure 3). Thus, we confirm that NaCl interference is not the cause of the observed near zero binding at pH 2 and 11.

Table S3. Average final concentrations of added HCl and NaOH to achieve the final solution pH

Final pH	[HCl] (mM)	[NaOH] (mM)
2	3.6±0.2	0
6	0	0.2±0.1
11	0	4.6±0.2

2. Additional Simulation Results and Discussion

2.1 Estimated Potential of Mean Force for Phosphate Micelle Binding

From the phosphate-micelle simulation at pH 6, we estimated the potential of mean force (PMF) profile as a function of separation distance between phosphates and the micelle center. The PMF is obtained *via* the equation $PMF(r) = kTln(P(r))$. The PMF profile shown is relative to the PMF at the distance of 8 nm, which corresponds to the unbound state. The PMF shows a minimum at a phosphate-micelle separation distance of approximately 3.5 nm. The PMF difference between this minimum and the unbound state is -11.6 kJ/mol.

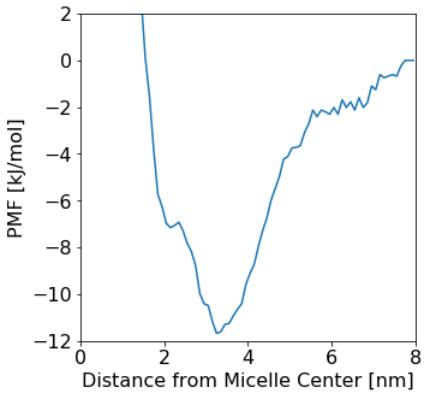

Figure S14. PMF as a function of the separation distance between phosphates and the micelle central axis. The result is obtained at the condition pH 11 and PA:PO_4 = 5:1.

2.2 Representative Snapshot of Multi-chain Binding

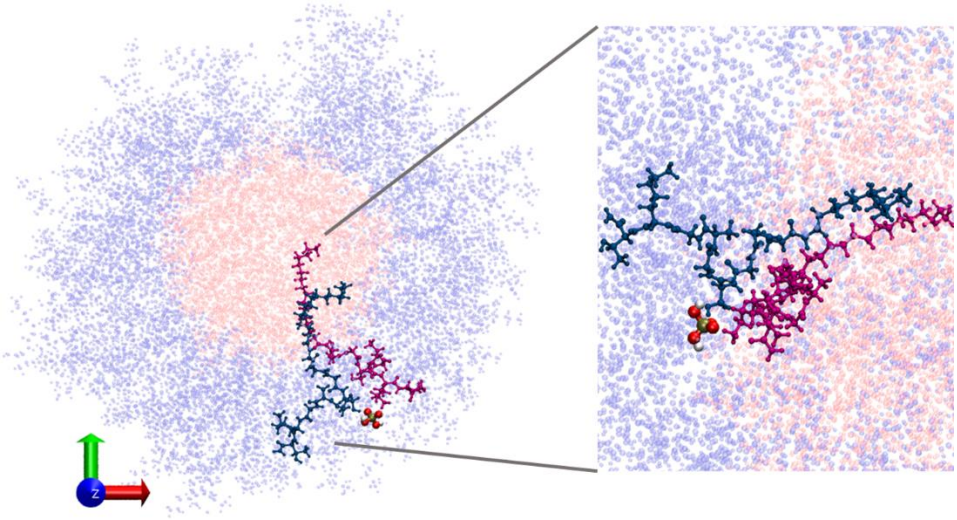

Figure S15. Representative snapshot of Multi-chain Binding from phosphate-micelle simulation at pH 6. The hydrophobic core is shown in red and the corona is shown in blue. The two different PA chains interacting with the phosphate is shown in dark blue and magenta, respectively.

3. Method and Materials

3.1 Synthesis and Purification of Peptide Amphiphile Micelles and Micelle Preparation Procedure

Two peptide sequences (GGGSGAGKT and SGAGKTSSSGGK(dde-protected)GGHHHSGAGKT) were synthesized on 0.25 mmoles of rink amide resin (Novabiochem) through standard FMOC solid phase peptide synthesis using an automated Prelude X Benchtop Synthesizer (Protein Technologies, Tuscon, AZ, USA). For each coupling step, the FMOC protecting group was first removed from the resin using 20% piperidine in dimethylformamide (DMF). Separately, the amino acid was activated with N,N,N',N'-Tetramethyl-O-(1H-benzotriazol-1-yl)uranium hexafluorophosphate (HBTU) and N,N-Diisopropylethylamine (DIPEA) in a molar ratio of 1:4:3.95:8 of resin: amino acid: HBTU: DIPEA. The activated amino acid cocktail was then added to the deprotected resin and then allowed to mix to conjugate.

After the amino acid couplings were completed, each peptide was then coupled with a palmitic acid tail. For the GGGSGAGKT peptide, the palmitic acid was simply conjugated to the deprotected glycine N-terminus. For the SGAGKTSSSGGK(dde-protected)GGHHHSGAGKT peptide, the palmitic acid was conjugated to the side chain of the 10^{th} residue lysine, ensuring first that the FMOC protecting group on the 1^{st} residue serine was not removed in the standard coupling procedure. The deprotecting cocktail for the dde-protecting group of the lysine was prepared by dissolving 1.8 mmol $NH_2OH.HCl$ and 1.35 mmol Imidazole in 5 mL N-Methyl-2-pyrrolidone (NMP), sonicating until dissolved. Just before adding the solution to the resin, Dichloromethane (DCM) was added in a 1:5 DCM to cocktail by volume proportion. The cocktail was then added to the resin and the solution was shaken for 3 hours to deprotect the side chain lysine. The solution was drained and washed with DCM and DMF. The palmitic acid was coupled to this free amine using the standard coupling cocktail described previously. After palmitic acid coupling, the FMOC of the serine was deprotected with 20% piperidine in DMF to leave a positively charged N-terminus.

After drying the resin under nitrogen, the peptide amphiphiles were then cleaved from the resin using a 95:2.5:2.5 by volume trifluoroacetic acid: triisopropylsilane: MilliQ water cleavage cocktail for 2 hours while shaking. The cleaved peptide amphiphiles were then precipitated through dropwise addition of the cleavage solution in a 50:50 by volume hexanes: -80 °C diethyl ether solution. The peptide amphiphiles were dried under nitrogen and dissolved in water.

The peptide amphiphiles were purified using reverse-phase HPLC (Prominence, Shimadzu, Columbia, MD, USA) on a C8 column (Waters, Milford, MA, USA) at 50 °C using acetonitrile and water with 0.1% formic acid as gradient mobile phases. The molecular weight of the products in the HPLC fractions were characterized by MALDI-TOF mass spectral analysis (Biflex III, Bruker, Billerica, MA, USA). The product-verified fractions were lyophilized and stored as powders at -20 °C. The purity was analyzed using a similar gradient method on an Agilent 6130 LCMS system in the University of Chicago's Mass Spectrometry Facility, using a Waters column, C8, XBridge, 4.6 mm × 150 mm, 5 μm particle size, and 130 Å pore size. The purity was calculated by integrating the area under the peaks during the elution time and dividing the area of the product peak by the area of all peaks, excluding peaks that were artifacts of the method. The purity was confirmed to be greater than 95% for both PAs.

Finally, the PA micelles were fabricated through dissolving the lyophilized powder in MilliQ water at the desired concentration, heating at 70 °C for 1 hour on a mechanical shaker, and letting the solution cool down and equilibrate at room temperature for at least 2 hours before experimental use.

3.2 Critical Micelle Concentration (CMC) Determination

The CMC was calculated by marking an increase of fluorescence intensity, corresponding to an increased micelle concentration, of a dissolved dye that fluoresces in the presence of hydrophobic micelle cores. To execute this experiment, 1,6-diphenyl-1,3,5-hexatriene (DPH) dye was dissolved in tetrahydrofuran at a concentration of 100mM and then diluted in water to a final concentration of 1 μM. Each PA was dissolved in 1 μM DPH solution and serially diluted by half to range from 0.001 μM to 1000 μM, performed in triplicates for each PA. The dilutions were allowed to equilibrate for one hour while covered with aluminum foil at room temperature. They were then transferred to a 96-well

plate in triplicates to minimize instrument error. Their fluorescence intensity was measured using a Tecan Infinite 200 plate reader (Mannedorf, Switzerland) with an excitation wavelength of 360 nm and an emission wavelength of 430 nm. The data were plotted with a log-transformed concentration and fit with two linear lines of best fit, one corresponding to the zero-slope portion and one fitting the data with increased fluorescence intensity. The CMC was identified as the intersection of these two fitted lines, approximating the inflection point of increased fluorescence intensity.

3.3 Negative-stain Transmission Electron Microscopy (TEM) Imaging

Carbon film 200 mesh copper grids were glow discharged with a Gatan Solarus plasma cleaning system for 30 s. They were then loaded with 3.5 μL of PAs for 1 minute, and then the excess was removed through blotting with filter paper. The grids were negatively stained with 0.75% uranyl formate for 45 s, blotted off to remove excess stain, and then were allowed to air dry before imaging. All transmission electron microscopy (TEM) imaging was performed on either the FEI Tecnai TF30 300 kV TEM (Hillsboro, OR, USA) or the FEI Tecnai Spirit 120 kV TEM (Hillsboro, OR, USA). The images were processed and measured digitally using ImageJ software, and the average dimensions were calculated from a sample size of at least 10 micelles.

3.4 Molybdenum Blue Assay for Analyzing Phosphate in Solution

To determine the amount of phosphate in solution, a spectrophotometric assay referred to as the molybdenum blue reaction was employed, which emits a blue color linearly proportional to the amount of phosphate present in solution. The reaction involves the following steps:

$$PO_4^{3-} + 12\ MoO_4^{2-} + 27\ H^+ \rightarrow H_3PO_4(MoO_3)_{12} + 12\ H_2O \qquad (1)$$

$$H_3PMo(VI)_{12}O_{40} + \text{reductant} \rightarrow [H_4PMo(VI)_8Mo(V)_4O_{40}]^{3-}. \qquad (2)$$

The first step consists of the reaction between phosphate, ammonium molybdate, and acid, producing a product that is then reduced in the second step to produce the final blue-colored product. Our procedure was modified from previous molybdenum blue assay designs.[3,4] For our procedure, the following reagents were prepared: 0.10 M ammonium molybdate (VI) tetrahydrate (ACS reagent, Acros Organics) in MilliQ water, 10%wt thiourea (99+%, for analysis, Acros Organics) in MilliQ water, 0.9 M sulfuric acid, and Na_2HPO_4 anhydrous (Fisher Scientific) in water at two concentrations of 1mM and 250 ppm phosphate. To conduct the assay for the calibration curve samples, 5 μL of ammonium molybdate, 10 μL of thiourea, and 5 μL of sulfuric acid were added in that order to 230 μL of a phosphate-containing solution with a concentration ranging from 0 to 50 ppm in MilliQ, diluted from the 250 ppm phosphate stock. Note that the reaction is catalyzed by acid, so the acid was added last and the time was recorded at this step to designate the start time of the reaction. The solution was vortexed and allowed to react for 45 minutes. Slightly before the reaction was completed, 75 μL of the molybdenum blue reaction solution was transferred in triplicates to a 96-well clear round-bottom plate. This was injected into a Tecan Infinite 200 plate reader (Mannedorf, Switzerland) so that it would be ready to be characterized precisely at the 45-minute mark. The spectrophotometric absorbance was measured at a wavelength of 700 nm and averaged between the three samples to minimize measurement error. The ammonium molybdate and phosphate stock solutions were recreated biweekly, to account for their shorter shelf life.

Each time this method was employed to derive the phosphate concentration of an unknown solution, a calibration curve with three samples of known phosphate concentration (0, 25, and 50 ppm) was created. A new curve was created each time to account for small fluctuations in absorbance depending on the age of reagents or time allowed to react. The data were fit with a linear line of best fit and were used the calculate the phosphate concentration of the unknown sample. The curve was rejected and recreated if the R-squared value was less than 0.99.

3.5 Analysis of pH-Dependent Phosphate Binding

The binding experiments consisted of combining PA and PO_4 solutions, adjusting the pH, physically separating the PA micelles from the solution with unbound phosphate, and analyzing the phosphate concentration of the filtrate. To perform a single measurement pH-dependent binding experiment, 62.5 μL of 1 mM Na_2HPO_4 stock was combined with 62.5 μL of a PA solution in MilliQ at a predetermined concentration to achieve the desired molar ratio of PA binding unit: PO_4, with a final phosphate concentration of 0.5mM for all binding experiments. Because C_{16}SGKGHhex has two binding units per molecule and C_{16}GGGhex only has one, the concentration of C_{16}SGKGHhex was half that of

C_{16}GGGhex to achieve the same molar ratio to phosphate. Upon combining the solutions, the pH was adjusted to the desired pH condition using minimal 0.25 M HCl and 0.25 M NaOH, vortexting between additions, and the pH was measured using a Fisher Scientific Accumet XL500 pH/ISE/Conductivity Benchtop Meter (Vernon Hills , IL, USA) and a Fisherbrand Accumet Micro Glass Mercury-Free Combination Electrode. Upon reaching the target pH, the PA/PO_4 solution was centrifuged at 9000 g^{-1} for 2 minutes to collect any viscous PA material that had accumulated on the side of the container, then transferred to a 1mL disposable pipette and filtered using a 13 mm 0.22 μm GHP Acrodisc syringe filter, collecting the filtrate sans PA in another vial. 75 μL of the filtrate was withdrawn and analyzed using proportional volumes of the spectrophotometric assay reagents (1.63 μL ammonium molybdate, 3.26 μL thiourea, and 1.63 μL sulfuric acid) and adhering to the rest of the assay protocol. For pH 2, 10, and 11 samples, the amount of added 0.25M NaOH and HCl for pH adjustment was recorded per sample, and the pH of each of the calibration point samples was adjusted to the same pH using an equivalent proportional volume of the NaOH and HCl that was added to the binding sample. The phosphate concentration of the assay sample was calculated using the calibration curve generated with each sample. The original phosphate concentration of the filtrate was then determined by accounting for the volume of the added spectrophotometric reagents which diluted the reading. This was repeated in duplicates or triplicates for each pH condition.

3.6 Analysis of Kinetics of Binding

This experiment was conducted similarly to the single measurement pH dependent binding experiments, but the total volume was increased to account for multiple samples being withdraw and multiple measurements taken. The total volume was calculated according to the following scheme: 125 μL * (number of samples) + 200 μL, with the last term ensuring that enough sample was retained. A solution of 5:1 ratio of C_{16}GGGhex to PO_4 at the desired volume was prepared such that the final concentration of PO_4 was 0.5 mM. The pH of the solution was adjusted using minimal HCl and NaOH to the desired pH condition. At each time point, beginning from the moment the desired pH was attained, the pH of the sample was recorded using Hydrion pH paper and 125 μL of solution was withdrawn, filtered, and analyzed as described previously.

3.7 Analysis of Selectivity over Nitrate and Nitrite

Samples were prepared in MilliQ in molar ratios of 1:1:1:1, 2:1:1:1, and 3:1:1:1 of PA:PO_4:NO_3:NO_2 equivalent to 10 ppm PO_4. The pH was adjusted and measured as previously described, and the solutions were mixed for 30 minutes to ensure the samples reached equilibrium in the more dilute regime. The samples were filtered as previously described to partition out the PA, and the filtrate was analyzed using ion chromatography.

Ion chromatography was preformed using a Thermo Scientific Dionex ICS-5000+ equipped with a Dionex AS-DV autosampler and using a Dionex IonPac AS22 column (Product No 064141, Thermo Scientific, California, USA). The analysis was run using an eluent of 4.5 mM Sodium Carbonate and 1.4 mM Sodium Bicarbonate (Product No 063965 from Thermo Scientific, California, USA) and a Dionex AERS 500 Carbonate 4 mm Electrolutically Regenerated Suppressor (Product No 085029 from Thermo Scientific, California, USA).

3.8 Analysis of Cycles of Capture and Release

The capture and release method was designed to simulate usage conditions of filtration through a packed bed reactor, collecting the released phosphate at designated release intervals. To simulate this, a 520 μL solution of C_{16}GGGhex and PO_4 was prepared in a 5:1 ratio such that the final concentration was 0.5 mM. To capture the phosphate, the pH was adjusted to pH 6 as described previously and left to equilibrate in a shake plate at 200rpm for 30 minutes. 500 μL of this solution was transferred to the filter compartment of an Amicon Ultra 0.5 mL 3K MWCO centrifugal filter and centrifuged for 4 minutes at 9,000 g^{-1}. This filtrate was analyzed using the spectroscopic assay as described previously. A new reclamation vial was switched out, and the retained PA was then washed with 200 μL Milli-Q water 6 times, centrifuging each time at the previous conditions, to ensure all unbound phosphate was removed from the dense PA suspension. The PA material was then recovered by inverting the filter compartment and collecting in a new collection vial by centrifuging at 1,000 g^{-1} for 10 minutes, or until all sample was recovered.

To perform the phosphate release and reclamation, 100μL of Milli-Q water was added to the filtration compartment and vortexed until well mixed with the PA. The now more dilute PA solution was transferred to a new binding analysis vial, and the total volume transferred was recorded. The volume of the recovered solution was raised to 480 μL using Milli-Q water, and the pH was adjusted to the desired release pH as previously described and left to equilibrate in a shake plate at 200rpm for 30 minutes. The amount of added acid and base was recorded. Upon reaching the target pH, Milli-Q water was added to reach a final volume of 500 μL. The released phosphate was then collected by transferring the solution to a centrifugal filter and centrifuging at 9,000 g^{-1} for 4 minutes. This filtrate was then analyzed using the spectrophotometric assay, adjusted for pH as previously described. The PA solution was washed as previously described. To prepare the solution for a recapture process, phosphate was added to the solution based on the amount of retained phosphate ions in the material as determined from the assay to obtain a 5:1 ratio of PA:PO_4 at a 0.5 mM concentration of PO_4 and a final volume of 500 μL. The solution was adjusted to pH 6, and the process was repeated as many times as desired.

3.9 Analysis of the Effect of NaCl on Binding and the Molybdenum Blue Assay

Samples were prepared in a 5:1 ratio of C_{16}GGGhex:PO_4 and varying NaCl concentrations such that the final PO_4 concentration was 0.5 mM and the final NaCl concentrations ranged from 2 μM to 40 μM. The samples were then adjusted to pH 6, filtered, and analyzed as described previously. To assess whether increased NaCl influences the reading of this assay, molybdenum blue calibration curves were constructed with varying amounts of NaCl added to match the final NaCl concentrations tested in the binding experiments. These curves were then compared to a standardized curve with no NaCl added.

3.10 Simulation Model and Force Field Parameters

Atomistic Model. The simulations used the GROningen MAchine for Chemical Simulations (GROMACS)[5] package and the ABF enhanced sampling methods implemented in SSAGES.[6] The PAs were modeled using the CHARMM forcefield[7] and water was modeled using the TIP3P model.[8] Custom force field parameters used for phosphate ions are listed in Tables S4-S7. The Lorentz-Berthelot mixing rule was used for unlike non-bonded interactions involving phosphate atoms. Nonbonded interactions were calculated using a 12 Å cutoff distance. Long-range electrostatic interactions were handled using fast smooth Particle-Mesh Ewald (SPME)[9] with a 0.12 nm Fourier spacing. Covalent bonds involving hydrogens were constrained using the LINCS algorithm.[10] All simulations were integrated using the leap-frog algorithm with a 2-fs timestep. All temperature-coupling used was Nosé–Hoover thermostat with a time constant of 0.1 ps used to maintain the temperature at 300 K.

Phosphate Force Field Parameters. Atom types in phosphate were assigned in the following way. In $H_2PO_4^-$, the phosphate atom is PMHP; the unprotonated oxygen atom is OPMH; OHMH and HOMH are the hydrogen atoms and the protonated oxygen atoms, respectively. In HPO_4^{2-}, the phosphate atom is PDHP; the unprotonated oxygen atom is OPDH; OHDH and HODH are the hydrogen atoms and the protonated oxygen atoms, respectively.

The nonbonded interactions include Lennard-Jones interactions and Coulombic interactions. For atoms i and j, their nonbonded interaction is:

$$u_{nb}(r_{ij}) = 4\epsilon_{ij}\left[\left(\frac{\sigma_{ij}}{r_{ij}}\right)^{12} - \left(\frac{\sigma_{ij}}{r_{ij}}\right)^{6}\right] + \frac{q_i q_j}{4\pi\varepsilon_0 r_{ij}}, \quad (1)$$

where r_{ij} is the separation distance between atoms i and j, σ_{ij} is the Lennard-Jones diameter, σ_{ij} is the Lennard-Jones interaction strength, ε_0 is the vacuum permittivity. q_i and q_j are the partial charges of atoms i and j. See Table S4 for nonbonded interaction parameters.

Table S4: Nonbonded interaction potential parameters for phosphate atoms.

atom	m (amu)	σ_{ii} (nm)	ϵ_{ii} ($\frac{\text{kJ}}{\text{mol}}$)	q (e)
PMHP	30.974	0.3296	0.6904	1.17
OPMH	15.999	0.2494	0.418	-0.91
OHMH	15.999	0.2672	0.418	-0.72
HOMH	1.008	0.04	0.192	0.28
PDHP	30.974	0.3296	0.6904	1.2
OPDH	15.999	0.2494	0.418	-0.78
OHDH	15.999	0.2494	0.418	-0.66
HODH	1.008	0.04	0.192	0.34

The 1-2 bonded atoms interact via a harmonic bonding potential in the form:

$$u_{bond}(r_{ij}) = \frac{k_{bond}}{2}\left(r_{ij} - {r_{ij}}^{(0)}\right)^2, \tag{2}$$

where r_{ij} is the separation distance between atoms i and j, k_{bond} is the force constant and ${r_{ij}}^{(0)}$ is the equilibrium bond length. The bonding interaction parameters are listed in Table S5.

Table S5: Bonding potential parameters for phosphate atoms.

bond	${r_{ij}}^{(0)}$(nm)	k_{bond} ($\frac{\text{kJ}}{\text{mol}\cdot\text{nm}^2}$)
PMHP-OPMH	0.154	485344
PMHP-OHMH	0.167	198322
OHMH-HOMH	0.0965	456056
PDHP-OPDH	0.154	485344
PDHP-OHDH	0.167	198322
OHDH-HODH	0.0965	456056

The 1-2-3 bonded atoms interact via a harmonic bending potential in the form:

$$u_{bend}(\theta_{ijk}) = k_{bend}\left(\theta_{ijk} - {\theta_{ijk}}^{(0)}\right)^2, \tag{3}$$

where k_{bend} is the force constant, θ_{ijk} is the angle between united atoms i, j, and k, and ${\theta_{ijk}}^{(0)}$ is the equilibrium angle. The bending interaction parameters are listed in Table S6.

Table S6: Bending potential parameters for polymer atoms.

Angle	${\theta_{ijk}}^{(0)}$(deg)	k_{bend} ($\frac{\text{kJ}}{\text{mol·rad}^2}$)
OPMH-PMHP-OPMH	114.23°	1004
OPMH-PMHP-OHMH	104.1°	827.6
PMHP-OHMH-HOMH	107.9°	836.8
OPDH-PDHP-OPDH	120°	1004
OPDH-PDHP-OHDH	108.7°	827.6
OHDH-PDHP-OHDH	102.9°	827.6
PDHP-OHDH-HODH	107.9°	836.8

The torsional potentials for 1-2-3-4 bonded united atoms take the form:

$$u_{tors}(\phi_{ijkl}) = k_{\phi}[1 + \cos(n\,\phi_{ijkl} - {\phi_{ijkl}}^{(0)})] \quad (4)$$

where k_{ϕ} is the coefficient and ϕ_{ijkl} is the dihedral angle defined by atoms i, j, k, and l. n is the integer multiplicity and ${\phi_{ijkl}}^{(0)}$ is a refence dihedral angle. The torsional interaction parameters are listed in Table S7.

Table S7: Bending potential parameters for polymer atoms.

dihedral	${\phi_{ijkl}}^{(0)}$(deg)	k_{ϕ} ($\frac{\text{kJ}}{\text{mol}}$)	n
OPMH-PMHP-OHMH-HOMH	0°	1.26	3
OHDH-PDHP-OHDH-HODH	0°	1.26	3
OPDH-PDHP-OPDH-HODH	0°	1.26	3
HODH-OHDH-PDHP-OPDH	0°	1.26	3

3.11 Simulations of Phosphate Binding to Single-Chain

Simulation Protocols. For the unbiased molecular dynamics simulations, a single C_{16}GGGhex chain and a single phosphate ion were placed in a cubic box (7 nm side length). At each pH condition, the phosphate ion was initialized at 9 different starting positions relative to the PA. For each replica, 20 ns of simulation under NVT ensemble in vacuum was performed to obtain a PA-phosphate bound structure. Then the system was solvated in water and a 10-ns NVT simulation for equilibration. Subsequently, another 10-ns MD trajectory under NVT ensemble was collected for analysis.

For ABF advanced sampling, two distance CVs identified in the cluster analysis, d_{SGAGKT} and d_{GGG}, were used to describe single-chain binding. Specifically, d_{SGAGKT} is defined as the distance between the center of mass of the phosphate and the center of mass of the following atoms:{Backbone N on 8GLY, backbone N on 9LYS, sidechain N on 9LYS, backbone N on 10THR, sidechain O on 10THR}. d_{GGG} is defined as the distance between the center of mass of the phosphate and the center of mass of the following atoms:{Backbone N on 2GLY, backbone N on 3GLY, O on 3GLY, backbone N on 5SER, and sidechain O on 5SER}. Note that the C_{16} region was counted as the first residue, and the following GGGSGAGKT peptide corresponded to residues 2-10. Each CV was bound within the interval [0.05 nm, 2.0 nm] and divided into 50 bins. Each ABF simulation used 4 parallel walkers under NVT ensemble. Restraints were placed foreach CV at values of 0.0 nm and 2.5 nm with a spring constant of 500 kJ mol^{-1} nm^{-2} to ensure that the configurations explored remained in the CV space of interest. For each ABF bin, a minimum visit of 400 was required before forces are

estimated. ABF was carried out and output monitored at intervals of 40 ns until the free energy features no longer changed between the two most recent outputs, resulting in 240 ns total simulation time per walker for both pH conditions.

Cluster Analysis. Cluster analysis was employed to identify the most frequently occurring PA-phosphate bound configurations. At each pH condition, snapshots from all nine trajectories were first rotationally and translationally aligned based on the peptide coordinates. Then the aligned snapshots were analyzed using the GROMACS cluster tool, using the gromos clustering algorithm[11] with a cutoff of 0.27 nm. The snapshots are clustered based on the peptide coordinates.

3.12 Simulations of Phosphate Binding to Peptide Amphiphile Micelle

Starting Configuration. The starting configuration for the PAM simulation was generated using a procedure in existing literature.[12] Briefly, nine PA molecules were packed in the *x*-*y* plane with the C_{16} tail pointing inwards, with 40° angle between adjacent chains. Then 24 layers were stacked in the *z*-direction with 20° offset and 5 Å distance between layers, resulting 216 PAs in total in the simulation box. Forty phosphate ions were inserted at random positions avoiding position overlap with the PA molecules. The simulation box was 16 nm in *x* and *y* direction (periodic) and 12 nm in *z* direction (non-periodic). The simulation box was solvated using the GROMACS solvate tool. Sodium (Na^+) or chloride (Cl^-) ions were added to neutralize the system.

Simulation Protocol. The starting configuration was energy-minimized using a steepest descent algorithm with a force tolerance of 10 kJ mol^{-1} nm^{-1} and a step size of 0.01 nm. The minimized configuration was then equilibrated under NVT ensemble for 4 ns. During this NVT simulation, for each PA chain, the position of the first carbon atom (closest to the micelle center) was restrained using a harmonic potential with a spring constant of 1000 kJ mol^{-1} nm^{-1} in each direction. Subsequently, the position restraint was removed, and the system was simulated for 50 ns under NPT ensemble, where the pressure in the *x*-*y* direction and the pressure in the *z* direction were coupled independently. For each direction, the pressure was maintained at 1.0 bar using Berendsen barostat with a time constant of 1.0 ps. Figure 5C displays the time evolution of the solvent accessible surface area (SASA) over the total 50-ns NPT trajectory, in which the SASA are shown to stabilize by 30 ns. As a result, the last 20 ns of MD trajectory was used for analysis.

Analysis. For hydrogen bond (H-bond) analysis, the GROMACS hbond tool was used to identify H-bonds formed between PA chains and phosphate ions. The H-bond criterion used a distance cutoff of 0.35 nm and an angle cutoff of 30°. Note that the GROMACS hbond tool uses the hydrogen-donor-acceptor angle instead of the donor-hydrogen-acceptor angle. The SASA was computed using the GROMACS sasa tool.[13] The entire micelle was selected for the SASA calculation.

3.13 Safety Comment

No unexpected or unusually high safety hazards were encountered during these experiments.

4. Author Roles and Responsibilities

All authors have read and approved the completed manuscript. W.C.F. led the design of the paper contents, coordinated the writing of the paper, and provided editorial oversight of the working manuscript. She performed the synthesis and purification of the PA micelles; conducted and analyzed the CMC experiments; performed TEM image acquisition and analysis; designed and conducted molybdenum blue assay experiments; designed, conducted, and analyzed pH-profile binding experiments; and designed and conducted selectivity experiments. She advised on the design of all subsequent binding experiments, and she analyzed all binding data. She wrote the entirety of the paper, excluding input for the simulation section. C.D. performed the molecular dynamics simulations of the micelle, and she wrote the simulation section of the manuscript. G.M.G. designed and conducted the molybdenum blue assay experiments. She designed, conducted, and analyzed binding experiments, including the pH-profile experiments, PA:PO_4 ratio binding experiments, kinetics of binding experiments, and both methods of capture and release

experiments. T.T. conducted and analyzed kinetics of binding, PA:PO_4 ratio binding experiments, capture and release experiments, and selectivity experiments. She designed, conducted, and analyzed the NaCl effect on binding experiments and the spectrophotometric assay. She also created the TOC graphic. A.Z.G. parameterized the phosphate force field and performed the molecular dynamics simulations of single-chain binding. M.Z. contributed to the design and implementation of the molybdenum blue assay and assisted with selectivity experiments. The corresponding authors M.G, J.J.d.P., and M.V.T. oversaw the manuscript direction, management, and submission as the principal investigators.

5. Supporting Information References

(1) Israelachvili, J. N.; Mitchell, D. J.; Ninham, B. W. Theory of Self-Assembly of Hydrocarbon Amphiphiles into Micelles and Bilayers. *J. Chem. Soc. Faraday Trans. 2* **1976**, *72*, 1525. https://doi.org/10.1039/f29767201525.

(2) Zhai, H.; Qin, L.; Zhang, W.; Putnis, C. V.; Wang, L. Dynamics and Molecular Mechanism of Phosphate Binding to a Biomimetic Hexapeptide. *Environ. Sci. Technol.* **2018**, *52* (18), 10472–10479. https://doi.org/10.1021/acs.est.8b03062.

(3) Nagul, E. A.; McKelvie, I. D.; Worsfold, P.; Kolev, S. D. The Molybdenum Blue Reaction for the Determination of Orthophosphate Revisited: Opening the Black Box. *Anal. Chim. Acta* **2015**, *890*, 60–82. https://doi.org/10.1016/j.aca.2015.07.030.

(4) Ganesh, S.; Khan, F.; Ahmed, M. K.; Velavendan, P.; Pandey, N. K.; Kamachi Mudali, U. Spectrophotometric Determination of Trace Amounts of Phosphate in Water and Soil. *Water Sci. Technol.* **2012**, *66* (12), 2653. https://doi.org/10.2166/wst.2012.468.

(5) Abraham, M. J.; Murtola, T.; Schulz, R.; Páll, S.; Smith, J. C.; Hess, B.; Lindah, E. Gromacs: High Performance Molecular Simulations through Multi-Level Parallelism from Laptops to Supercomputers. *SoftwareX* **2015**, *1–2*, 19–25. https://doi.org/10.1016/j.softx.2015.06.001.

(6) Sidky, H.; Colón, Y. J.; Helfferich, J.; Sikora, B. J.; Bezik, C.; Chu, W.; Giberti, F.; Guo, A. Z.; Jiang, X.; Lequieu, J.; et al. SSAGES: Software Suite for Advanced General Ensemble Simulations. *J. Chem. Phys.* **2018**, *148* (4). https://doi.org/10.1063/1.5008853.

(7) Vanommeslaeghe, K.; Hatcher, E.; Acharya, C.; Kundu, S.; Zhong, S.; Shim, J.; Darian, E.; Guvench, O.; Lopes, P.; Vorobyov, I.; et al. CHARMM General Force Field: A Force Field for Drug-like Molecules Compatible with the CHARMM All-Atom Additive Biological Force Fields. *J. Comput. Chem.* **2009**, *32* (4), 671–690. https://doi.org/10.1002/jcc.21367.

(8) Jorgensen, W. L.; Chandrasekhar, J.; Madura, J. D.; Impey, R. W.; Klein, M. L. Comparison of Simple Potential Functions for Simulating Liquid Water. *J. Chem. Phys.* **1983**, *79* (2), 926–935. https://doi.org/10.1063/1.445869.

(9) Essmann, U.; Perera, L.; Berkowitz, M. L.; Darden, T.; Lee, H.; Pedersen, L. G. A Smooth Particle Mesh Ewald Method. *J. Chem. Phys.* **1995**, *103* (19), 8577–8593. https://doi.org/10.1063/1.470117.

(10) Hess, B.; Bekker, H.; Berendsen, H. J. C.; Fraaije, J. G. E. M. LINCS: A Linear Constraint Solver for Molecular Simulations. *J. Comput. Chem.* **1997**, *18* (12), 1463–1472. https://doi.org/10.1002/(SICI)1096-987X(199709)18:12<1463::AID-JCC4>3.0.CO;2-H.

(11) Daura, X.; Gademann, K.; Jaun, B.; Seebach, D.; van Gunsteren, W. F.; Mark, A. E. Peptide Folding: When Simulation Meets Experiment. *Angew. Chemie Int. Ed.* **1999**, *38* (1/2), 236–240. https://doi.org/10.1002/(sici)1521-3773(19990115)38:1/2<236::aid-anie236>3.3.co;2-d.

(12) Lee, O. S.; Stupp, S. I.; Schatz, G. C. Atomistic Molecular Dynamics Simulations of Peptide Amphiphile Self-Assembly into Cylindrical Nanofibers. *J. Am. Chem. Soc.* **2011**, *133* (10), 3677–3683. https://doi.org/10.1021/ja110966y.

(13) Eisenhaber, F.; Lijnzaad, P.; Argos, P.; Sander, C.; Scharf, M. The Double Cubic Lattice Method: Efficient Approaches to Numerical Integration of Surface Area and Volume and to Dot Surface Contouring of Molecular Assemblies. *J. Comput. Chem.* **1995**, *16* (3), 273–284. https://doi.org/10.1002/jcc.540160303.